The Journal of Neuroscience, September 1990, 10(9): 2996–3013

Ultrastructural Localization of Tyrosine Hydroxylase in the Rat Ventral Tegmental Area: Relationship Between Immunolabeling Density and Neuronal Associations

Virginia E. Bayer and Virginia M. Pickel

Division of Neurobiology, Department of Neurology and Neurosciences, Cornell University Medical College, New York, New York 10021

Dopaminergic neurons of the A10 cell group in the rat ventral tegmental area (VTA) exhibit electrical and dye coupling. Also, the activity of these neurons at least partially reflects their content of tyrosine hydroxylase (TH), the rate-limiting enzyme in catecholamine biosynthesis. We examined the ultrastructural localization of TH to determine the morphological features of dopaminergic neurons in the VTA and the relationships between their TH immunoreactivity content and afferent input. Antiserum against the trypsin-treated form of TH was localized using peroxidase–antiperoxidase (PAP) and immunoautoradiographic methods. Immunoreactivity was detected in perikarya, dendrites, and terminals. The perikarya contained the usual organelles, as well as cilia, lamellar bodies, and subsurface cisterns. Qualitative evaluation of peroxidase reaction product and quantitative analysis of the number of silver grains/unit area revealed varying amounts of TH immunoreactivity in nuclei and cytoplasm. Lightly or intensely labeled nuclei were not necessarily associated with corresponding cytoplasmic labeling density. However, cytoplasmic labeling directly corresponded to the relative frequencies of neuronal appositions and synaptic input. Those neurons with less dense cytoplasmic PAP product received fewer synaptic contacts and were less frequently in apposition to other TH-labeled soma and dendrites than neurons displaying relatively more dense cytoplasmic PAP product. Analysis of single sections revealed that 67% (n = 71) of all TH-labeled somata and 15% (n = 2431) of all TH-labeled dendrites were in apposition to other TH-labeled soma or dendrites. TH-labeled terminals were rarely detected and contained relatively low levels of immunoreactivity. The majority of labeled terminals (n = 29/46) formed synapses with labeled soma and dendrites. Unlabeled terminals (n = 2424) in contact with TH-labeled dendrites appeared to form predominantly symmetric synapses. Ten percent (n = 248) of the unlabeled terminals dually synapsed onto adjacent immunoreactive dendrites, perikarya, or dendrite and perikaryon. We conclude that in the rat VTA, (1) detected TH immunoreactivity in cytoplasm, but not nucleus, corresponds to the level of feedback principally from non-dopaminergic afferents; (2) dendrodendritic as well as axodendritic synapses between TH-immunoreactive neurons may mediate dopaminergic autoinhibition; and (3) gap junction-like appositions between neurons and convergent inputs from unlabeled terminals onto TH-immunoreactive profiles provide an anatomical substrate whereby cellular activities might be coordinated under certain conditions.

Dopaminergic neurons of the A-10 group (Dahlstrom and Fuxe, 1964) in the ventral tegmental area (VTA) are well characterized with respect to anatomical connectivity and function. They project to and receive input from limbic and cortical structures (Oades and Halliday, 1987) involved in central regulation of locomotor activity (Mogenson et al., 1979), motivation (Papp and Bal, 1986), brain stimulation reward (Crow, 1972), and selective attention (Simon et al., 1980; Piazza et al., 1988). The cytoplasmic localization of the catecholamine-synthesizing enzyme tyrosine hydroxylase (TH) has been demonstrated in neurons of the VTA by both light and electron microscopy (Hökfelt et al., 1976; Herve et al., 1987; Vincent, 1988). However, the ultrastructural studies were limited to one labeling method and did not explore the detailed ultrastructural features of these neurons, the possible noncytosolic localization of TH, or the relationship between density of immunoreactivity for TH and synaptic input or dendritic associations. We addressed these issues using immunoperoxidase and immunoautoradiographic labeling for TH in the adult rat VTA. The results have implications for synaptic regulation and for junctional coupling (Grace and Bunney, 1983) of dopaminergic neurons via convergent synaptic input and gap-like junctions. We also established a cellular basis for catecholaminergic modulation in VTA via dendrodendritic and axodendritic synapses between TH-labeled neurons.

Materials and Methods

Antiserum. Antiserum against TH was generously supplied by Dr. Tong H. Joh. This antiserum was produced in rabbits by previously described methods (Joh and Ross, 1983). Specificity of the antibody was shown by formation of a single immunoprecipitate with purified antigen, by selective inhibition of TH activity, and by the absence of immunocytochemical labeling with antiserum pretreated with excess antigen.

Tissue preparation. Ten adult male Sprague-Dawley rats (200–250 gm) were anesthetized with sodium pentobarbital (50 mg/kg, i.p.), then perfused through the ascending aorta with 10 ml heparinized saline, 50 ml of 3.75% acrolein in 2% paraformaldehyde in 0.1 M phosphate buffer

Received Jan. 3, 1990; revised Mar. 12, 1990; accepted Apr. 26, 1990.

We gratefully acknowledge our debt to Dr. Tong H. Joh for supplying the TH antiserum and to June Chan for her tremendous technical expertise. We would also like to acknowledge the helpful suggestions on this study by Drs. G. P. Smith and T. H. Joh. This research was supported by NIMH grants MH00078 and MH40342 and NIDA DA04600.

Correspondence should be addressed to V. Bayer, Department of Neurobiology and Neurosciences, Division of Neurobiology, Cornell University Medical College, 411 East 69th Street, New York, NY 10021.

(pH 7.4). The brains were removed, cut into 1 mm coronal slices, and postfixed in 2% paraformaldehyde for 30 min. Coronal vibratome sections, 30–40 μm thick, were collected in 0.1 M phosphate buffer through the rostrocaudal extent of the VTA. Vibratome sections were then incubated in 1% sodium borohydride in phosphate buffer for 30 min to cross-link aldehydes (Abdel-Akher et al., 1952), rinsed in phosphate buffer, and transferred to 0.1 M Tris-saline for subsequent immunolabeling either with peroxidase–antiperoxidase (PAP) or immunoautoradiography as outlined below.

PAP labeling. Vibratome sections from 6 rats were sequentially processed through a series of incubations adapted from Sternberger (1979). These include (1) 1:2000 dilution of TH antiserum for 24 hr, (2) three 15 min washes, (3) 1:100 dilution of goat anti-rabbit immunoglobulin for 30 min, (4) three 15 min washes, (5) 1:100 dilution of rabbit PAP (Sternberger-Meyer, Jarretsville, MD). Steps 2–5 were then repeated (after Ordronneau et al., 1981) and the tissue washed 3 times for 15 min. All dilutions and washes were performed in 0.1 M Tris-saline (pH 7.6) at room temperature and under constant agitation. Sections were reacted with a solution of 22 μg 3,3′-diaminobenzidine and 10 μl 30% hydrogen peroxide in 100 ml Tris-saline for 6 min to visualize the peroxidase reaction product (Sternberger, 1979). Sections for light microscopy were mounted onto gelatin-coated slides, dehydrated, and coverslipped. Tissue for electron microscopy was processed as outlined below.

Immunoautoradiographic labeling. Vibratome sections from 4 rats were immunoautoradiographically labeled using the method described by Pickel et al. (1986). The steps included (1) 1:2000 dilution of TH antiserum for 24 hr, (2) three 15 min washes, (3) 1:50 dilution of ^{125}I-labeled donkey anti-rabbit immunoglobulin (Amersham, Arlington Heights, IL) with a specific activity of 100 μCi/ml for 2 hr, (4) one 10 min wash, (5) 30 min washes repeated until negligible radioactivity was detected in the wash solutions. All dilutions and washes were prepared in 0.1 M Tris-saline (pH 7.6). All incubations and washes were carried out at room temperature and under constant agitation. Sections used for light microscopy were mounted onto gelatin-coated slides, defatted in chloroform/ethanol, rehydrated, dipped in Ilford L4 emulsion, and exposed in light-proof boxes for 5–7 d. Slides were developed in Kodak D-19, fixed with Kodak Ektaflo, rinsed, dehydrated, and coverslipped. Tissue for electron microscopy was processed as outlined below.

Processing for electron microscopy. Sections labeled by both PAP and immunoautoradiographic methods were fixed for 2 hr in 2% OsO4 in 0.1 M phosphate buffer, rinsed twice in phosphate buffer, dehydrated, and flat embedded in Epon 812. These were subsequently embedded in Epon in capsules, and ultrathin sections were collected from the outer surface of the tissue. In PAP-labeled tissue, sections were put on copper grids and counterstained with lead citrate and uranyl acetate. In immunoautoradiographically labeled tissue, ultrathin sections were deposited by a loop onto parlodion-coated slides. The slides were counterstained, carbon-coated, dipped in Ilford L4 emulsion, and exposed in light-proof boxes for 4–6 months. The slides were subsequently developed with Kodak Microdol-X, rinsed, fixed in 30% sodium thiosulfate, and washed. The parlodion was floated off the slides, the sections collected on nickel grids, the parlodion removed, and the sections analyzed. The autoradiographic procedure for electron microscopy was adapted from Beaudet and Descarries (1986). All analysis was performed on a Phillips 201 electron microscope.

Numerical sampling procedure. PAP-labeled tissue from 3 rats was used in the analysis. In each case, 2 grids containing several ribbons of ultrathin sections were examined for both the parabrachial pigmentosus and paranigral subdivisions of the VTA at the level of, or just anterior to the entry of the 3rd cranial nerve (Paxinos and Watson, 1986). No significant differences were seen between the 2 subdivisions; thus, they were combined into a single analysis. Within each grid, dendritic profiles were sampled from 3 squares of a randomly picked section. The squares were chosen on the basis of nearness of tissue to the surface of the block. This ensured labeling of TH-immunoreactive terminals which were difficult to detect except at the surface of the tissue. Only 1 grid from each region was used to compile statistical data since only 1 grid per pair was analyzed for dendritic size in addition to input and associations. Thus, 2431 dendrites were analyzed. Within a given square, dendritic profiles were detected 135 times as frequently as somatic profiles. Somatic profiles, therefore, were counted within the entire section to ensure adequate numbers for further analysis. Somatic profiles included both sections through nuclei and large regions of cell bodies where the nucleus was not transected.

Quantification of reaction product. Peroxidase reaction product was qualitatively assessed on the basis of observed electron density relative to neighboring profiles. Thus, neurons were evaluated as intensely or lightly immunoreactive exclusively on the basis of comparisons between pairs of labeled profiles. In immunoautoradiographic preparations (4 rats), the number of silver grains/μm^2 of cytoplasm or nucleus was evaluated. Adjacent neurons were broadly subdivided into more heavily or more lightly immunoreactive based upon comparison of number of silver grains/area. The same type of analysis was used for nuclei, with the comparison being made relative to the amount of labeling in the cytoplasm of the same cell. Analyses between samples were only conducted after cells within samples were subdivided with respect to their relative density of labeling.

Results

The perikarya and processes immunolabeled for TH had identical morphological characteristics when examined by both peroxidase and immunoautoradiographic labeling methods. Thus, light microscopy results are jointly described. The ultrastructural observations complement each other, with PAP providing easier detection and immunoautoradiography providing a more quantitative measure of immunoreactivity.

Light microscopy

Morphology and distribution patterns were consistent with previous reports (Phillipson, 1979a, b) for both labeling methods employed. TH labeling was seen in the paranigral, parabrachial pigmentosus, interfascicular, and rostral and caudal linear nuclei (Fig. 1*a*). Subdivisions are based upon the nomenclature of Paxinos and Watson (1986). Pairs of TH-immunoreactive perikarya were commonly detected throughout the VTA (Fig. 1*b*). Labeled perikarya exhibited a wide range of density in cytoplasmic immunoreaction product (Fig. 1*c*). Nuclei of immunoreactive soma also were sometimes labeled for TH. These displayed a range of labeling densities which did not appear related to the levels of cytoplasmic immunoreactivity. Nuclei of unlabeled cells did not show similar immunoreactivity. Adjacent TH-immunoreactive processes were frequently seen (Fig. 1*c*).

Electron microscopy

The parabrachial pigmentosus and the paranigral subdivisions of the VTA were examined by electron microscopy. As numerical analyses of both regions provided similar results, the 2 regions were combined in subsequent analyses.

Labeling in perikarya and dendrites. In sections collected from the surface of the tissue, qualitative assessment of peroxidase product and quantitative analysis of silver grains/μm^2 revealed a range of labeling densities in nuclei and cytoplasm of neuronal perikarya.

Nuclei containing TH-like immunoreactivity (THLI) were detected only within perikarya displaying cytoplasmic labeling for the enzyme. These nuclei were characterized by variabilities in (1) electron density attributed to counterstaining, (2) indentations of their nuclear envelopes, and (3) density of immunoreaction product for TH. The density of nuclear immunoreactivity was not correlated with either of the first 2 variables, nor was it correlated with the density of cytoplasmic labeling for TH in the same neuron. The outer leaflets of the nuclear membrane of TH-immunoreactive perikarya appeared in many cases to be labeled more strongly than the surrounding cytoplasm (Fig. 2*a*, open arrows).

The differences in cytoplasmic labeling densities were suffi-

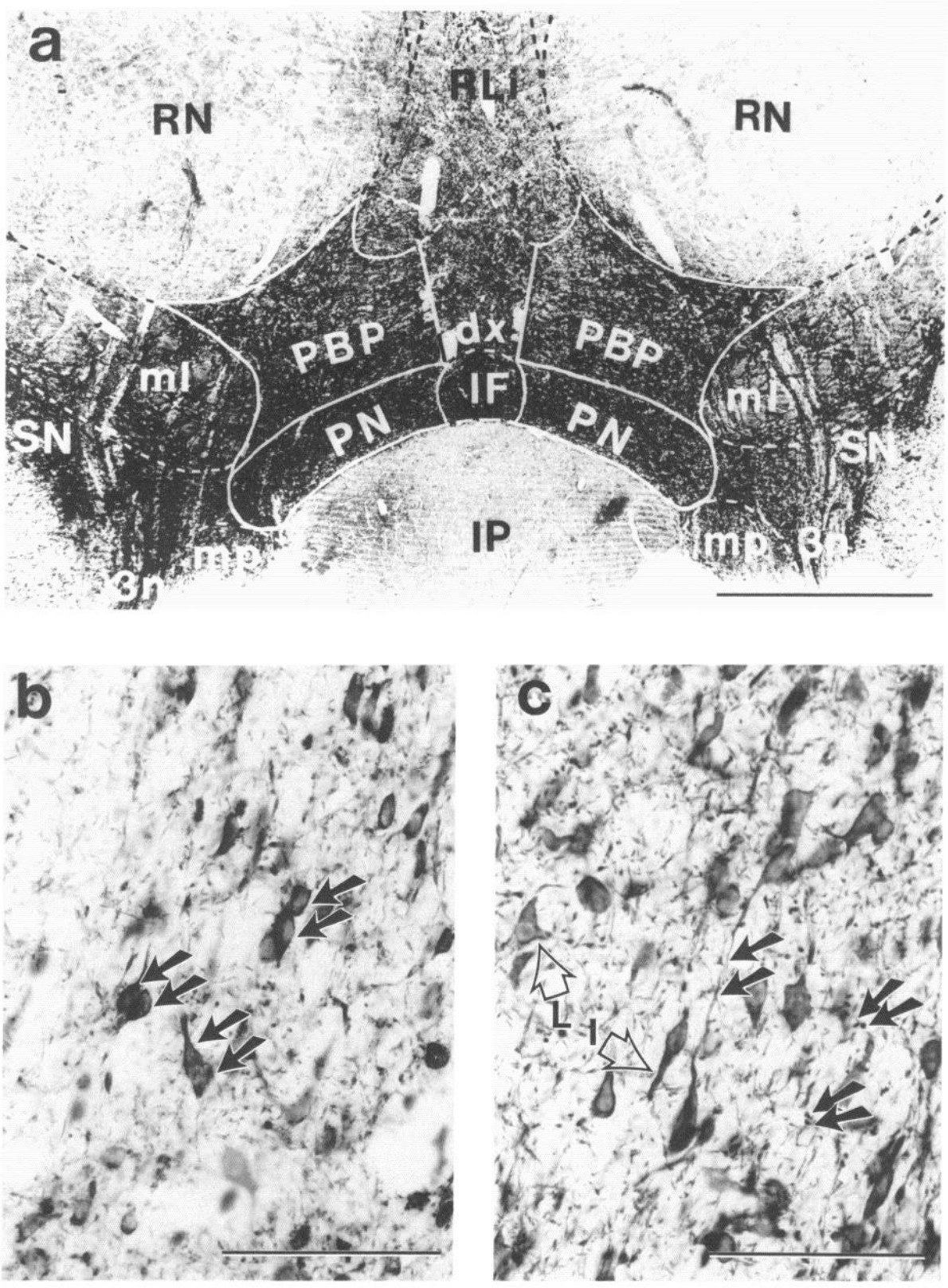

Figure 1. Light micrographs of ventral tegmental area (VTA) immunostained with antibody to tyrosine hydroxylase, visualized by the peroxidase–antiperoxidase method. *a,* Photomicrograph of a coronal section through the ventral tegmental area at the level of the third cranial nerve showing dense TH labeling in the parabrachial pigmentosus subnucleus (*PBP*), paranigral subnucleus (*PN*), interfascicular subnucleus (*IF*), rostrolinear subnucleus (*RL*) and region around ventral tegmental decussation (*dx*). Regions surrounding the VTA: *SN,* substantia nigra; *RN,* red nucleus; *ml,* medial lemniscus; *mp,* mammillary peduncle; *3n,* 3rd cranial nerve; *IP,* interpeduncular nucleus. *b,* Photomicrograph (parabrachial pigmentosus) showing pairs of apposed TH-labeled perikarya (*arrows*). *c,* Photomicrograph (paranigral) showing apposed TH-labeled processes (*closed arrows*). *Open arrows* point to intensely labeled cell (*I*) and lightly labeled cell (*L*). Scale bars, 4 mm in *a,* 100 μm in *b* and *c.*

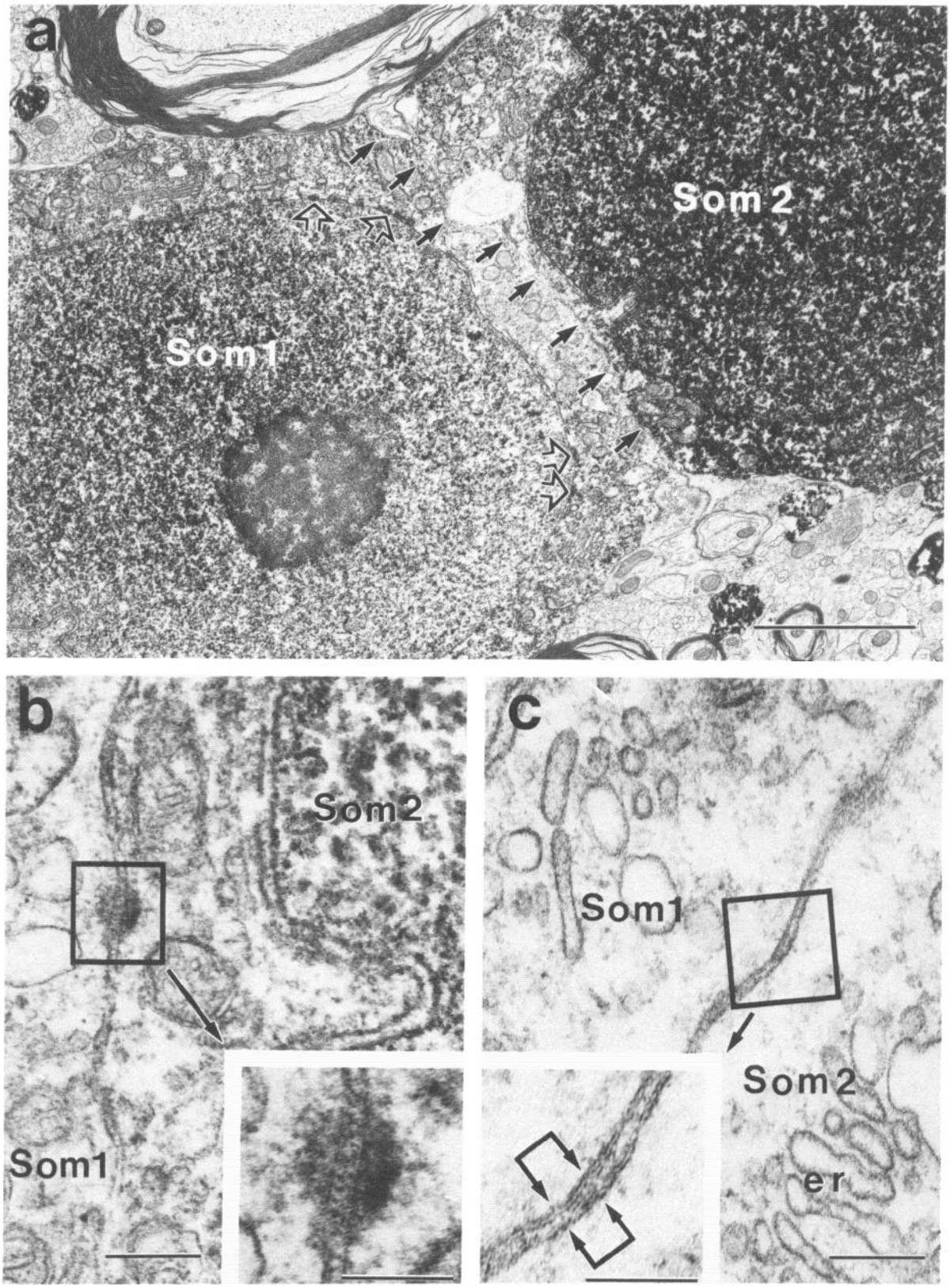

Figure 2. Apposed perikarya show junctional specializations and different densities of peroxidase. *a,* Electron micrograph revealing differing densities of PAP product in nuclei and cytoplasm of 2 soma (Som 1 and Som 2); *closed arrows,* border between adjacent cell bodies; *open arrows,* sections of nuclear envelope showing labeling for TH. *b,* Electron micrograph of a nonadjacent serial section to section *a* showing detail of cell–cell border with puncta adherens-like structure (*box*); *inset of box* shows filamentous plaques on either side of cell–cell border and structural regularity between the 2 plaques. *c,* Electron micrograph of a section taken at a distance of approximately 10 μm further through the same pair of cells shown in *a.* Gap junction-like appositional zone in boxed area is shown at a high magnification in inset. Border region between arrows shows laminated appearance of junctional zone; *er,* smooth endoplasmic reticulum. Scale bars, 2.0 μm in *a,* 0.2 μm in *b* and *c,* 0.1 μm in insets.

Table 1. Immunoautoradiographic labeling for tyrosine hydroxylase: comparison of cytoplasmic or nuclear densities in 6 pairs of somata

	Silver grains/μm^2				Ratio of cytoplasmic grains[a] (A/B)	Cytoplasm/nucleus ratio	
	Cell A		Cell B				
Pair	Cytoplasm	Nucleus	Cytoplasm	Nucleus		Nucleus A	Nucleus B
1	9.27	7.33	3.15	1.50	2.94 (I/L)[b]	1.26	2.10
2	0.33	4.83	7.57	5.75	1.10 (L/L)[c]	1.73	1.32
3	14.82	10.13	10.42	8.39	1.42 (I/I)	1.46	1.24
4	15.86	9.03	9.51	1.49	1.67 (I/L)	1.76	6.38
5	33.13	11.16	22.38	9.49	1.39 (I/I)	2.79	2.30
6	9.73	4.91	4.29	1.52	2.27 (I/L)	1.99	2.82

[a] Ratio of number of silver grains/μm^2 of cytoplasm versus nucleus. Ratio > 2.00 = light, ratio < 2.00 = intense.

[b] An intense (I) and lightly (L) immunoreactive pair is defined by the ratio A/B > 1.5.

[c] Pairs with A/B < 1.5 are defined either as both light or both intense according to their position on a variability scale, from lowest (3.15) to highest (15.86) number of silver grains/μm^2 cytoplasm, with pairs previously defined (A/B > 1.5) used as guidelines.

ciently large to permit distinction of groups of perikarya and dendrites with low or high detected levels of TH immunoreactivity. The following staining patterns were noted: (1) both cytoplasm and nucleus were lightly immunoreactive (Fig. 2*a*, som 1), or intensely immunoreactive (Fig. 2*a*, som 2), or (2) a combination of either intensely immunoreactive cytoplasm with lightly immunoreactive nucleus or lightly immunoreactive cytoplasm with intensely immunoreactive nucleus. In PAP-labeled material, 75% (53/71) of soma were classified as intensely immunoreactive on the basis of their cytoplasmic labeling, without regard to nuclear labeling. The differing densities of immunoreactivity found in the cytoplasm of the perikarya extended well into their dendritic branches (Fig. 3*c*), where 72% (1735/2431) were intensely labeled. Semiquantitative analysis of immunoautoradiographically labeled material showed differences in numbers of silver grains ranging from 3–31 grains/μm^2 soma (n = 12). Although variable, concentration of silver grains between matched pairs from the same sample yielded results similar to those of PAP-labeled material; namely, that a majority of cells (58%) could be classified as intensely immunoreactive (see Table 1).

Somal Attachment Sites. In PAP-labeled material, perikarya and dendrites immunoreactive for TH were followed through numerous serial sections until a sufficient depth from the surface was reached to allow for clear visualization of the appositional zone (compare Figs. 2*a*, 3*a*). This was not necessary for immunoautoradiographic labeling because there was less obstruction of subcellular detail by silver grains versus peroxidase product. Several types of attachments were seen between adjacent TH-containing perikarya. These included puncta adherens-like attachments (Fig. 2*b*). Filamentous plaques were seen on both sides of the attachment zone, with electron-dense bands spanning the plasmalemmas and forming a regular array between the plaques. In other regions of appositions between TH-labeled perikarya, the plasmalemmas narrowed and had a laminar appearance (Fig. 2*c*). The space separating the 2 plasmalemmas of cells immunoautoradiographically labeled for TH also frequently appeared fused or laminated. However, the border between the cells could also become widely separated and indistinct. Direct somatosomatic appositions were only noted between labeled somata. In cases where a TH-labeled soma and unlabeled soma were adjacent to one another, a glial membrane appeared to separate them. Appositions between a labeled soma and labeled dendrites occurred more than twice as often as between a labeled soma and unlabeled dendrites (Table 2). Analysis of pairs of TH-labeled soma showed membrane-bound saccules in close proximity to the appositional zone. These saccules were 50–200 nm in length and were either smooth or had a coating of amorphous material (Fig. 3*b*, small arrow). In some instances, the saccules appeared to be fused with the plasma-

Table 2. Average number of dendritic contacts[a] per section through lightly vs intensely TH-immunoreactive soma and dendrites

	Unlabeled dendrite		Labeled dendrite	
	Lightly immunoreactive	Intensely immunoreactive	Lightly immunoreactive	Intensely immunoreactive
Soma[b]	0.22 (4/9)	0.28 (15/53)	0.72 (13/18)	0.57 (30/53)
Dendrites[c]				
Large	0.33 (2/6)	0.06 (2/36)	0.00 (0/6)	0.31 (11/36)
Medium	0.07 (27/396)	0.05 (57/1191)	0.017 (68/396)	0.16 (192/1191)
Small	0.03 (10/294)	0.02 (8/508)	0.13 (39/294)	0.06 (33/508)

[a] Sizes of dendrites were as follows: small, <0.5 μm; medium, 0.5–1.5 μm; large, >1.5 μm, in cross-sectional diameter.

[b] Dendritic contacts include appositions with and without membrane specializations.

[c] Soma refers to profiles containing nuclei (n = 32) and large sections of cell bodies where the nuclei were not transected (n = 39).

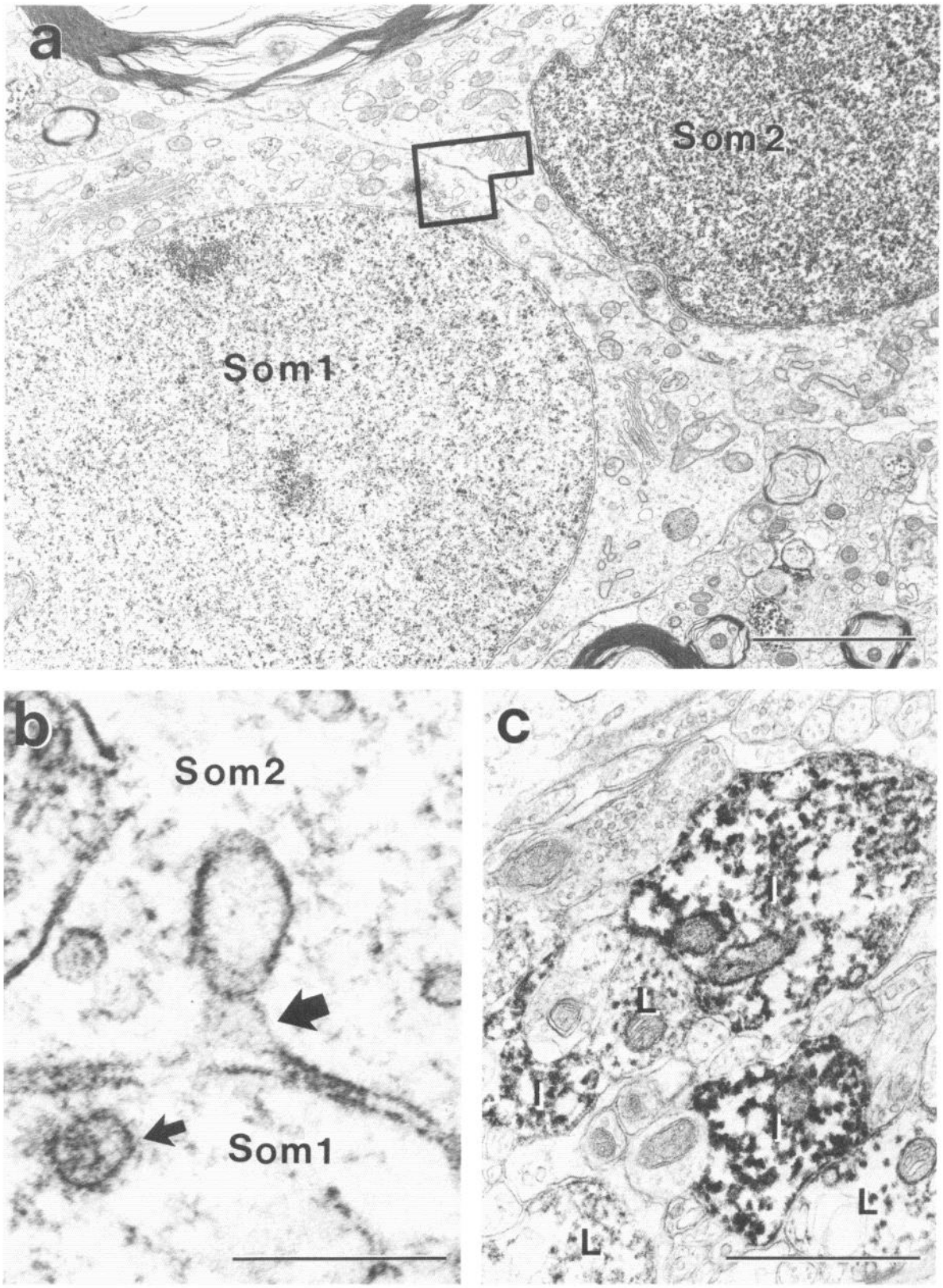

Figure 3. Electron micrographs of same 2 cell bodies (*Som 1, Som 2*) as in Figure 2, but lacking immunoreactivity for TH due to greater depth of section from surface of the tissue. *a,* Low-power micrograph; *boxed area* shows region magnified for Figure 2*c*. *b,* Nonadjacent serial section showing saccule apparently fused with cell membrane (*large arrow*); what appears to be a coated saccule is also nearby (*small arrow*). *c,* Section taken near surface of block showing differences in immunoreactivity of adjacent dendrites (*I,* intensely immunoreactive; *L,* lightly immunoreactive). Scale bar, 2.0 μm in *a,* 0.2 μm in *b,* 1.0 μm in *c*.

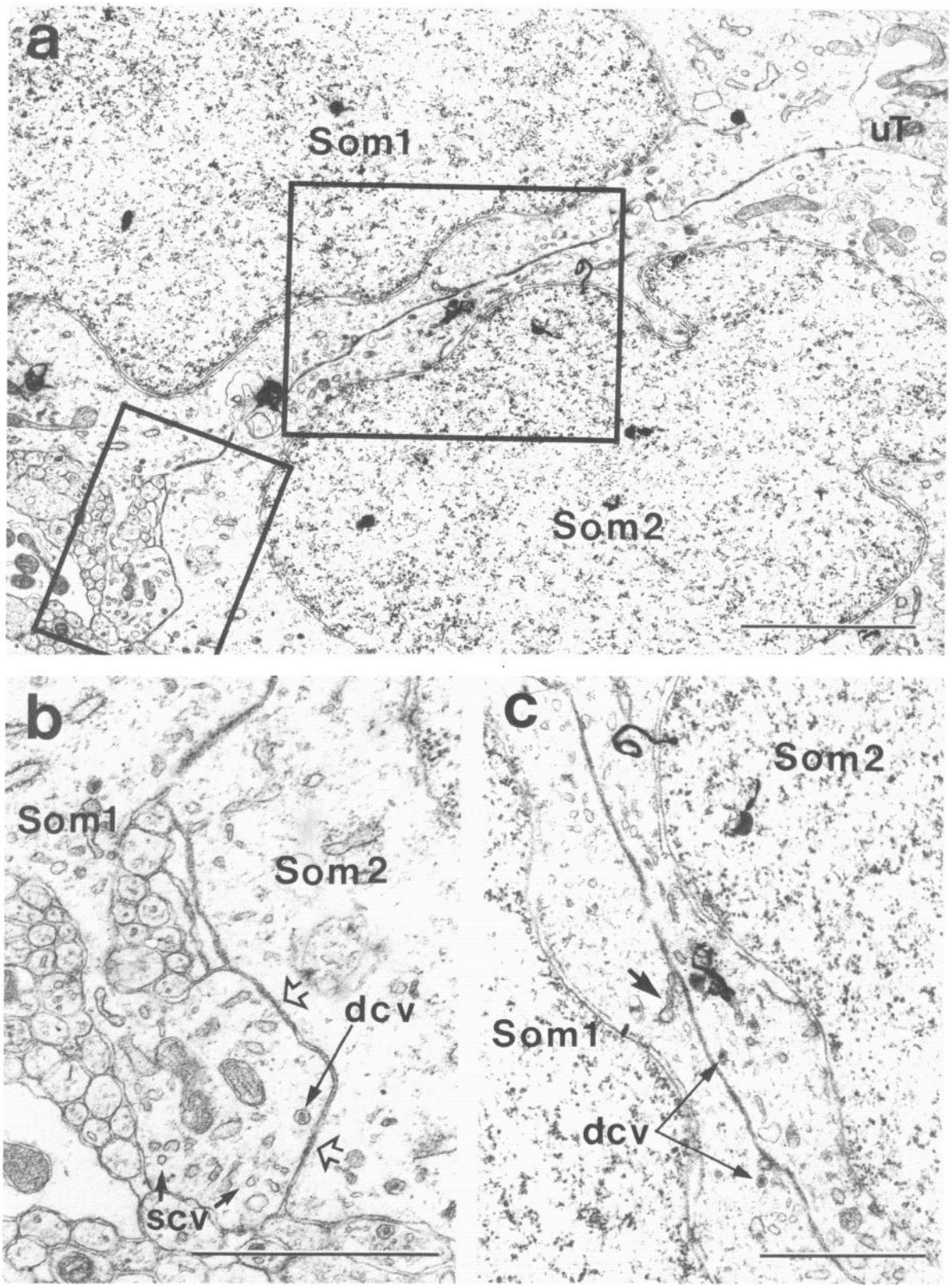

Figure 4. Apposed plasmalemmas of cell bodies immunoautoradiographically labeled for TH. *a,* Electron micrograph showing silver grains over cytoplasm and nuclei of Som 1 and 2; unlabeled terminal (*uT*) is in contact with both cells. *Boxed areas* are shown in higher magnification. *b,* From box on left in *a.* A cytoplasmic extension from soma 1 is in direct contact with soma 2. Contact areas (*open arrows*) are similar in size and density to junctions between soma. *dcv,* dense-core vesicle; *scv,* smooth clear vesicles. *c,* From box on right in *a.* Apposed somatic plasmalemmas are flanked by saccular structures (*large arrow*) and dense-core vesicles (*dcv*). A thin rim of cytoplasm separates the apposed plasmalemmas from the nuclei. Scale bar, 2.0 μm in *a,* 1.0 μm in *b* and *c.*

lemma along the border between 2 cells (Fig. 3*b*, large arrow). Smooth endoplasmic reticulum (Fig. 2*c*) and, on occasion, dense-core vesicles were also seen near the appositional zone. In immunoautoradiographically labeled material, coated saccules were seen in the vicinity (Fig. 4*c*, arrow) of these somal attachments. The nuclei of attached TH-labeled perikarya were usually eccentrically located and positioned near the cell–cell border (Fig. 4*c*).

TH-labeled neurons often had one or more somatic and dendritic spines, and occasionally exhibited more unique processes. Apposed TH-labeled somata (Fig. 4*a*, 5*a*) sometimes showed cytoplasmic protrusions extending from one neuron into (Fig. 5*b*) or onto (Fig. 4*b*) the other. Two such protrusions were noted on one pair of apposed neurons. The first appeared to extend into the cytoplasm of the apposed cell and had a granular appearance (Fig. 5*b*), while the second one emerging from the same soma abutted its neighbor at the cell surface (Fig. 4*b*). The latter protrusion contained mitochondria, smooth endoplasmic reticulum-like saccules and even a dense-core vesicle. The apparent junctions made by this extension (open arrows) have characteristics similar to those seen between adjacent perikarya.

Synaptic input to soma. TH-labeled perikarya received synaptic input principally from unlabeled terminals (362/369). Most unlabeled terminals formed symmetric synapses with 1 or sometimes 2 TH-labeled perikarya within a single plane of section. The density of synaptic input to a given perikaryon ($n = 32$) in single section analysis varied from 1–23 terminals/soma and was correlated with detected cytoplasmic immunoreactivity for TH. Intensely TH-immunoreactive perikarya received almost twice as many synapses as lightly TH-immunoreactive perikarya (Table 3). Dual synaptic contacts from unlabeled terminals to 2 TH-labeled perikarya were frequently seen. These contacts were either symmetric or asymmetric. Synaptic contacts on both soma were sometimes seen within a single section (Fig. 5*c*, arrows). Postsynaptic elements known as Taxi bodies (Taxi, 1961) seen in certain types of asymmetric synapses were also detected (Fig. 5*c*, small arrows).

Cytoplasmic organelles. Organelles were most evident between cells examined at a level where PAP reaction product was no longer an obstacle to analysis (as in Fig. 3*a*). The most commonly observed organelles included ribosomes, rough and smooth endoplasmic reticulum, Golgi, lysosomes, and mitochondria. TH-immunoreactive cells additionally contained a number of more unusual organelles, including lamellar bodies (Fig. 6*b*), subsurface cisterns (Fig. 6*a*), and cilia (Fig. 6, *c*, *d*). Lamellar bodies, made up of circularly arranged layers of smooth endoplasmic reticulum, were most often found as single structures, but perikarya with multiple lamellar bodies were not uncommon. The central core of the lamellar bodies could either be empty or contain dense-core vesicles. Subsurface cisterns, also made up of stacks of smooth endoplasmic reticulum, were seen immediately beneath the plasmalemma. A glial process was usually found opposite the cistern on the external surface of the cell. Cilia extended from the cytoplasm into the surrounding neuropil and were characterized by a 9+0 microtubule arrangement proximally and 8+1 distally. Basal bodies (Fig. 6*c*) and ciliary rootlets also were observed. One cilium appeared to penetrate a TH-labeled perikaryon, as in this case it was encircled by a double plasma membrane. These organelles were seen in sections immunolabeled by both PAP (Fig. 6, *b*, *d*) and immunoautoradiographic (Fig. 6, *a*, *c*) methods and could occur in either soma or dendrites of both lightly and intensely immunoreactive perikarya. A few cells also contained more than one type of unusual organelle seen within a single plane of section.

Table 3. Average number of contacts from unlabeled terminals per section through lightly vs intensely TH-immunoreactive soma and dendrites

	Lightly immunoreactive	Intensely immunoreactive
Soma[a]	3.67 (66/18)	5.45 (289/53)
Dendrites[b]		
Large	2.00 (12/6)	2.56 (92/36)
Medium	1.00 (395/396)	1.15 (1364/1191)
Small	0.20 (60/294)	0.29 (146/508)

[a] See Table 2, footnote *a*.

[b] See Table 2, footnote *b*.

[c] Statistically significant ($p > 0.05$) increases in contacts per section onto intensely relative to lightly labeled profiles.

Dendrites: PAP and immunoautoradiographically labeled. Dendrites resembled perikarya in terms of variability in immunoreactivity for TH and variety of cytoplasmic organelles. The description, therefore, will focus on types of dendritic interactions and their synaptic input.

Somatic and dendritic associations. TH-containing dendrites were often either apposed to a TH-containing perikaryon or dendrite or apposed to both a labeled perikaryon and dendrite (Fig. 7*a*). Smooth, clear vesicle-like structures, approximately 20–50 nm in diameter, sometimes accumulated on the somatic side (Fig. 7*b*). Additionally, smooth endoplasmic reticulum was seen in the somatic cytoplasm immediately adjacent to the appositional zone. At high magnifications, the plasmalemmal boundaries between TH-labeled soma and dendrites or between 2 labeled dendrites usually had characteristics similar to those found between apposed TH-containing perikarya (Figs. 3*c*, 7*c*). Appositions between unlabeled soma and TH-labeled dendrites resembled those seen when 2 TH-labeled soma were apposed, their plasmalemmas being in similarly close contact.

Rarely, TH-labeled dendrites were in contact with either labeled or unlabeled dendrites showing prominent membrane specializations comparable to axodendritic synapses (Fig. 8). Within an unlabeled dendrite, which gave a view unobstructed by PAP product, the junctional thickening extended throughout the length of the appositional zone (Fig. 8*a*). Contacts with recognized membrane specializations also were seen between 2 TH-labeled dendrites (Fig. 8*b*). These densities also appeared to span the length of the appositional zone. Vesicles were not detected within the dendrites on either side of the dendritic junctions. Dendritic associations were most frequently seen between 2 intensely immunoreactive dendrites (65/99) but were also detected between intense and more lightly labeled dendrites (27/99) and between 2 lightly labeled dendrites (7/99). Apposed dendrites were postsynaptic to at least one axon terminal.

Synaptic input from unlabeled terminals. Forty-nine percent of TH-labeled dendrites ($n = 2431$) received contacts from one or more identifiable terminals within a single section. Of these, 98% of the junctions were from terminals lacking TH immunoreactivity. This analysis included TH-labeled dendrites with cross-sectional diameters ranging from 0.2–2.5 μm. From a sample of 2424 unlabeled terminals, 10% formed synapses with more than one TH-labeled profile within a single plane of section. Unlabeled terminals appeared to form both symmetric and

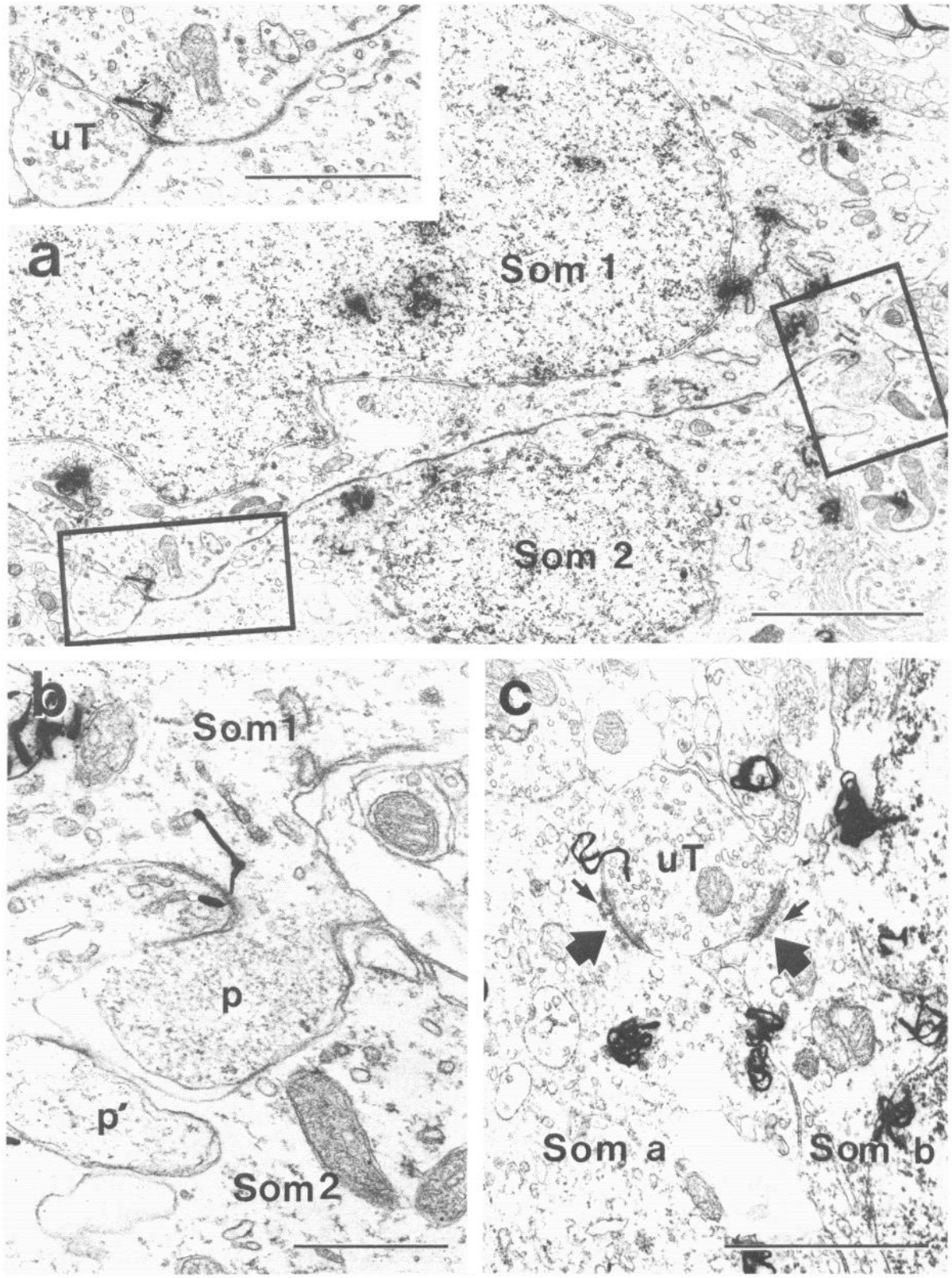

Figure 5. Synaptic input and extensions of apposed cell bodies (*Som 1* and *Som 2*) immunoautoradiographically labeled for TH. *a,* Electron micrograph of nonadjacent serial section of perikarya from Figure 4. *Inset* of region outlined in lower left of *a* shows an unlabeled terminal (*uT*) in contact with both cell bodies. *b,* Higher magnification of area outlined in lower right of *a* showing process (*p* and *p'*) from soma 1 penetrating into or overlapping soma 2; cytoplasm of process has a granular appearance. *c,* Unlabeled terminal (*uT*) making asymmetric synaptic contacts (*big arrows*) with 2 apposed TH-labeled perikarya (*Som a* and *Som b*); note Taxi bodies (*small arrows*) below postsynaptic densities. Scale bar = 2.0 μm in *a,* 0.5 μm in *b,* 1.0 μm in *c* and *insert.*

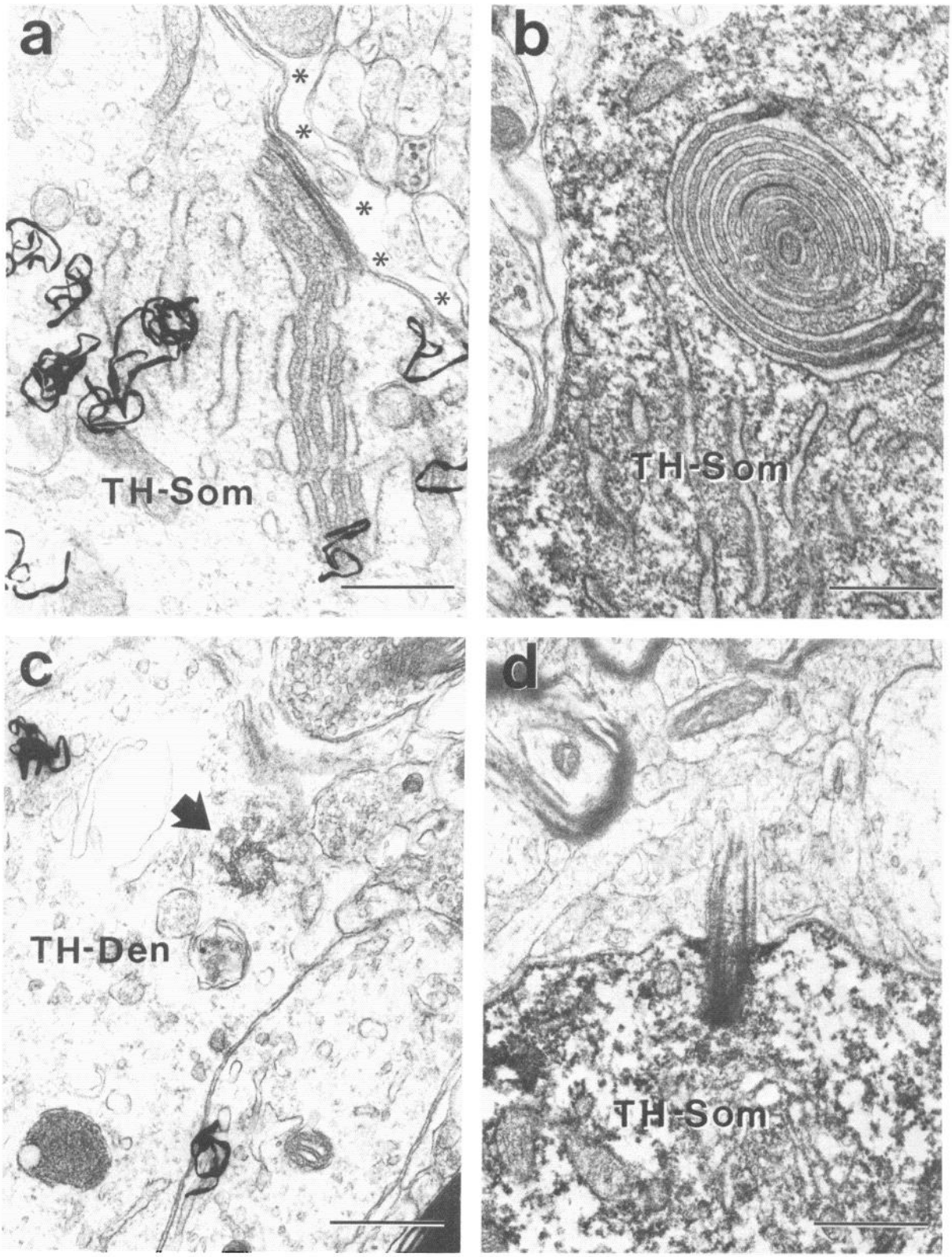

Figure 6. Micrographs of unusual subcellular organelles in TH-labeled soma and dendrites. *a,* Immunoautoradiographically labeled TH soma (*TH-Som*) containing a subsurface cistern at its border with a glial process (*asterisks*). *b,* PAP labeling for TH in a soma (*TH-Som*) with lamellar body. *c,* Immunoautoradiographically labeled TH dendrite (*TH-Den*) with cilium (*arrow*) in cross-section at basal body. *d,* PAP-labeled TH-immunoreactive soma (*TH-Som*) with cilium in sagittal section protruding into neuropil. Scale bar, 0.5 μm throughout.

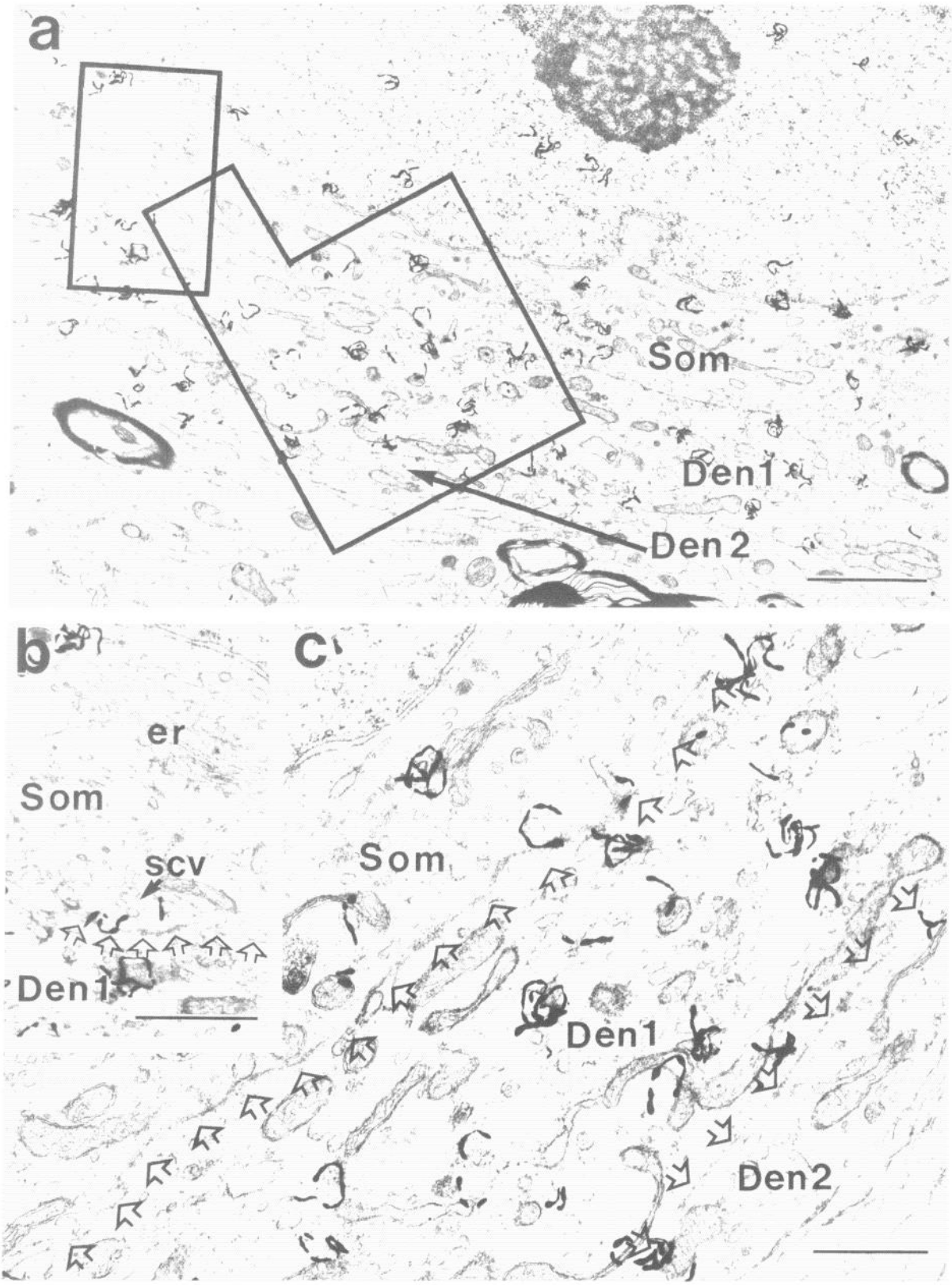

Figure 7. Direct apposition between a soma and dendrite immunoautoradiographically labeled for TH. *a*, Electron micrograph showing extensive region of contact between TH-labeled soma (*Som*) and TH-labeled dendrite (*Den 1*). A second TH-labeled dendrite (*Den 2*) is in direct apposition to the first dendrite. Numerous silver grains are superimposed over the cytoplasm of the soma and dendrites; a few grains are also over the nucleus, but there are none over the nucleolus or surrounding neuropil. *b*, Magnification of region outlined in *a* showing smooth endoplasmic reticulum and/or smooth clear vesicles (*scv*) in the border region between the soma and Den 1 (*open arrows*); *er*, smooth endoplasmic reticulum. *c*, Magnification of region outlined in *a* showing apposed plasmalemmas between the cell soma and dendrite 1 and between dendrites 1 and 2 (*open arrows*). Scale bar, 1.0 μm in *a*, 0.5 μm in *b* and *c*.

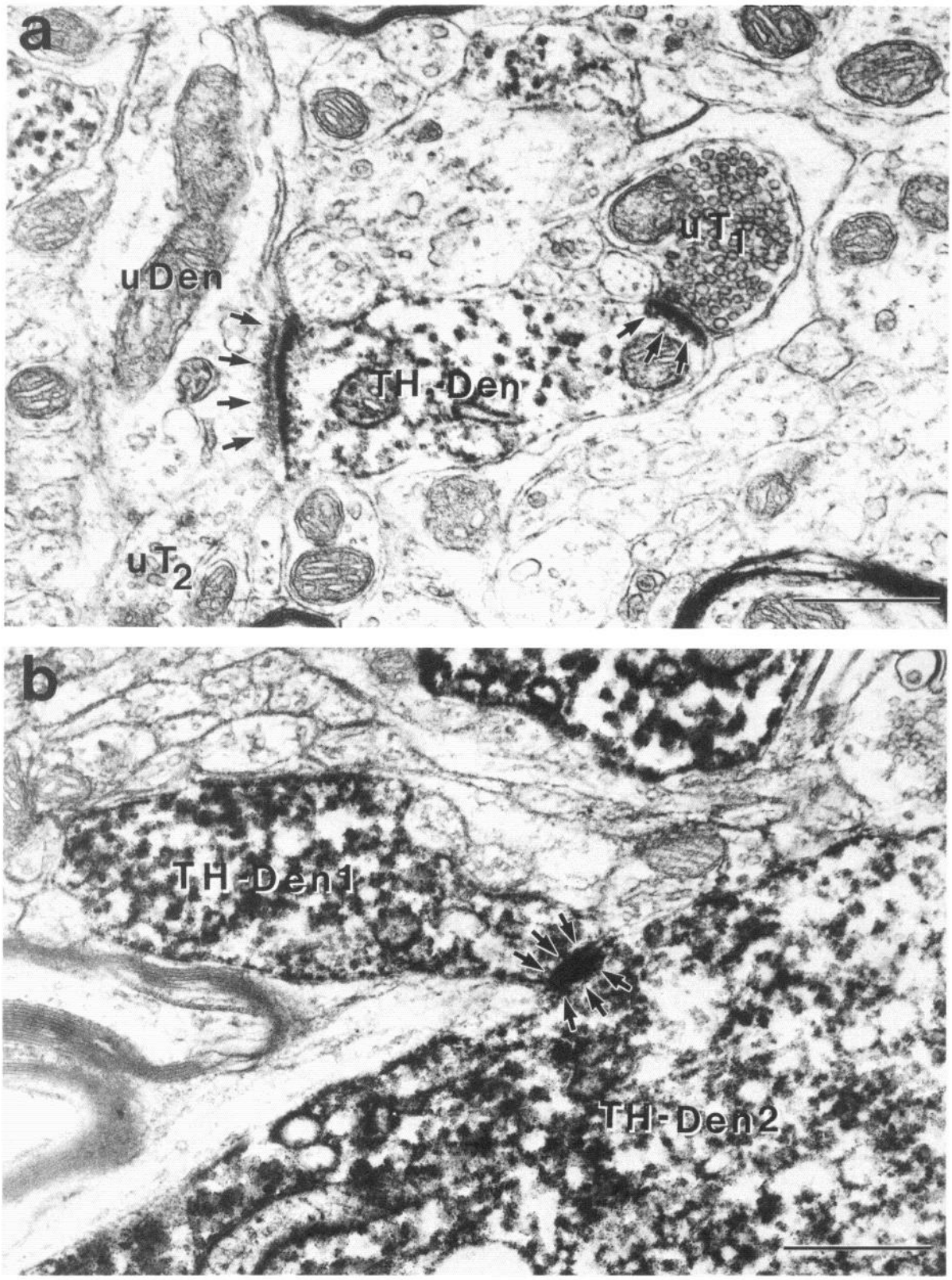

Figure 8. TH labeling in dendrites showing junctions with other unlabeled or labeled dendrites. *a,* Electron micrograph of TH-labeled dendrite (*TH-Den*) in contact with both an unlabeled terminal (*uT-1*) and an unlabeled dendrite (*u Den*); thick membrane specializations (*arrows*) are seen at both contact points; uT-1 lacks the granularity associated with PAP labeling despite being more electron dense than other unlabeled terminals (*uT-2*). *b,* Dense contact specialization (*arrows*) between 2 TH-labeled dendrites (*TH-Den 1* and *TH-Den 2*). Scale bar, 0.5 μm in *a* and *b*.

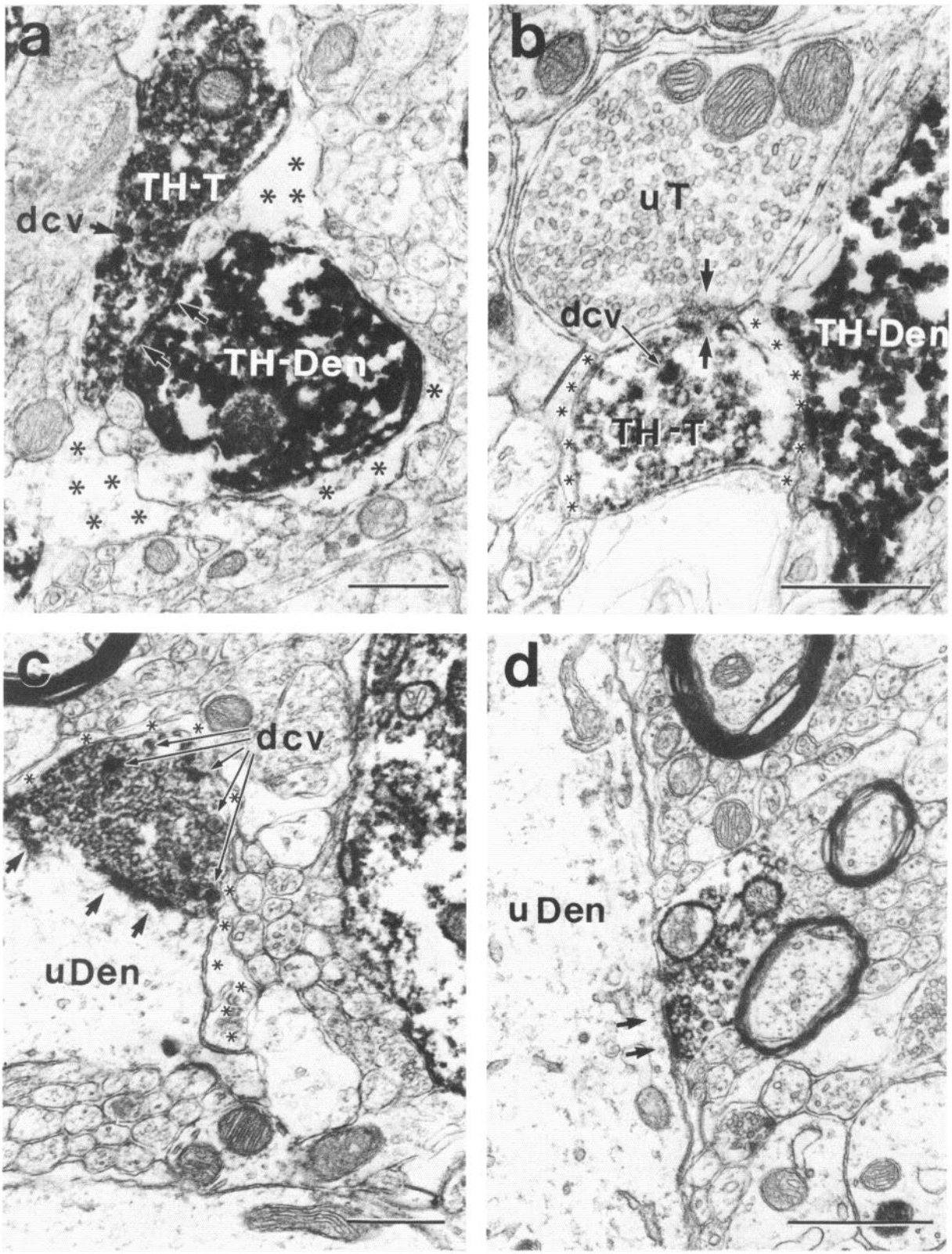

Figure 9. PAP-labeled TH-immunoreactive terminals. *a,* Electron micrograph showing TH-labeled terminal (*TH-T*) making an apparent synaptic contact (*arrows*) with a TH-labeled dendrite (*TH-Den*); *asterisks,* glial processes; *dcv,* dense-core vesicle. *b,* TH-labeled terminal in apposition, displaying dense membrane specialization (*arrows*), with an unlabeled terminal (*uT*); a nearby TH-labeled dendrite (*TH-Den*) is separated from the TH-labeled terminal by an intervening glial process (*asterisks*); *dcv,* dense-core vesicle. *c,* TH-labeled terminal forming asymmetric synapse (*arrows*) with unlabeled dendrite (*u DEN*); *dcv,* dense-core vesicles; *asterisks,* glia. *d,* TH-labeled terminal making symmetric synapse (*arrows*) with unlabeled dendrite (*u Den*). Scale bar, 0.5 μm in *a–d.*

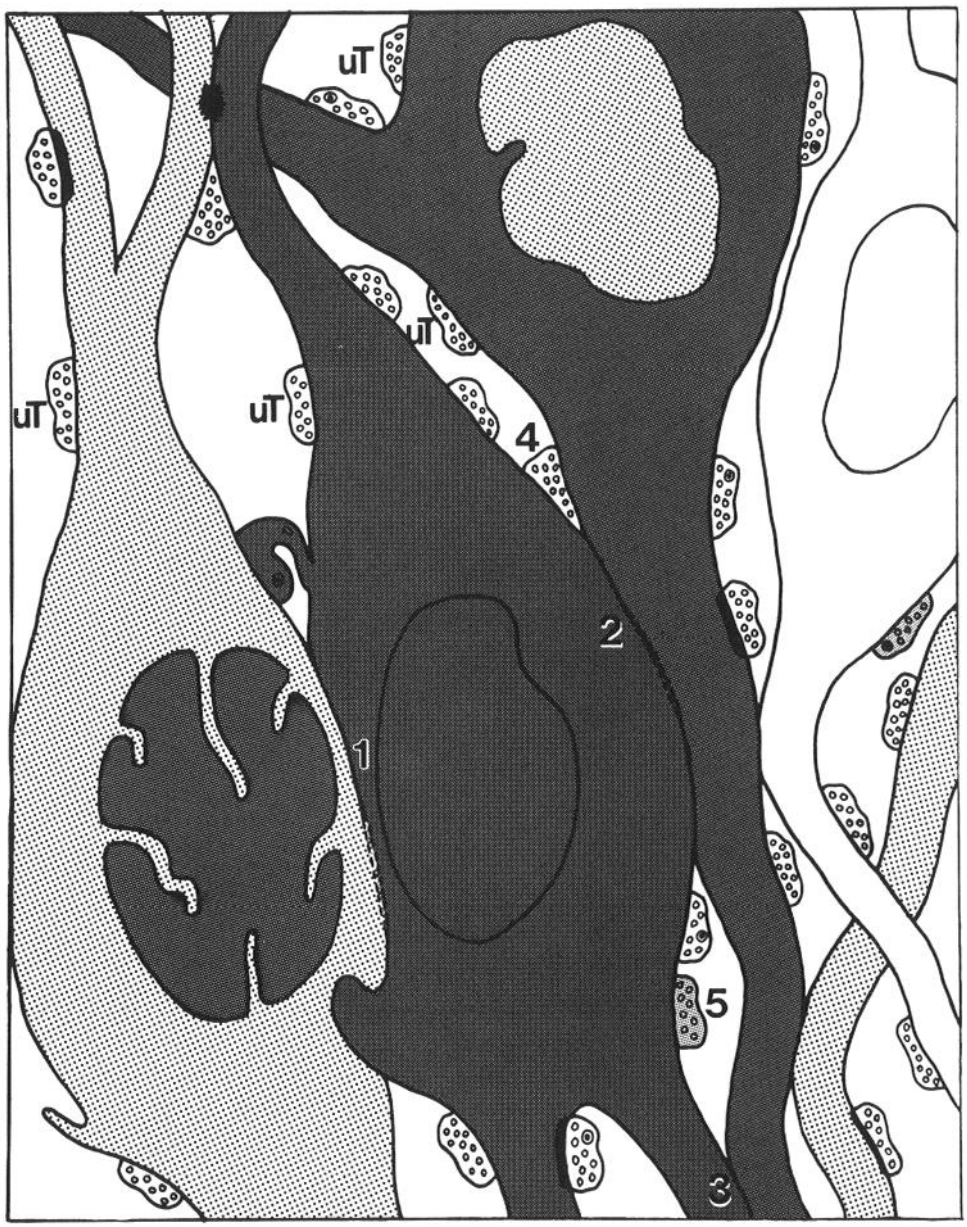

Figure 10. Summary schematic showing major findings on ultrastructural localization of TH in the rat VTA. Perikarya with intense cytoplasmic labeling for TH (*dark shading*) receive more numerous contacts from unlabeled terminals (*uT*) than perikarya with lightly immunoreactive cytoplasm (*light shading*). Relative numbers of synapses on perikarya with unlabeled cytoplasm (*unshaded*) were not analyzed. Intensity of nuclear labeling is not correlated with intensity of cytoplasmic labeling as indicated by *shading*. Somatosomatic (*1*), somatodendritic (*2*), and dendrodendritic (*3*) appositions were most common between 2 neurons with intensely labeled cytoplasm. Dual inputs (*4*) were also more common between profiles displaying intense cytoplasmic immunoreactivity. Synapses are seen between TH-labeled terminals and labeled (*5*) and unlabeled dendrites.

asymmetric junctions, with the majority being of the symmetric type. However, sampling at the surface to ensure adequate labeling of all TH-immunoreactive terminals often resulted in dense peroxidase products that obscured postsynaptic densities.

Dual symmetric input similar to that seen between 2 TH-labeled perikarya were also seen between apposed soma and dendrites. Of the 104 unlabeled terminals making dual contacts, 65 joined 2 intensely TH-immunoreactive dendrites, while 7 joined 2 lightly TH-immunoreactive dendrites. Twenty-seven joined one lightly labeled and one unlabeled dendrite, while only 4 synapsed on a labeled dendrite/soma pair.

Synaptic input from TH-labeled terminals. Even with the more easily recognized peroxidase product, terminals immunoreactive for TH were much less intensely labeled and less numerous ($n = 46$) than either TH-containing perikarya ($n = 71$) or dendrites ($n = 2431$). These terminals usually contained mitochondria, numerous smooth clear vesicles approximately 30–40 μm in diameter and often one or more large 80–100 μm dense-core vesicles (Fig. 9*c*). Reaction product usually rimmed both small and large vesicles, though the central core of some dense core vesicles also appeared immunoreactive. Dense-core vesicles were most often located away from the synaptic junctions.

Sixty-three percent (29/46) of the TH-labeled terminals directly contacted TH-containing perikarya and dendrites without glial separation (Fig. 9*a*). However, many perikarya and dendrites were so heavily labeled with PAP product for TH that appositions versus synaptic junctions were not always distinguishable. TH-labeled terminals were never observed in contact with other TH-labeled terminals. Seven of 29 TH-immunoreactive terminals synapsed upon intensely immunoreactive soma ($n = 53$), while none contacted lightly immunoreactive soma ($n = 18$). Nineteen TH-labeled terminals contacted intensely immunoreactive medium or small dendrites ($n = 1699$) and 3 contacted lightly labeled medium or small dendrites ($n = 690$). No TH-labeled terminals were detected in apposition to proximal dendrites containing TH immunoreactivity. The re-

maining 37% (17/46) of TH-immunoreactive terminals formed synapses with unlabeled dendrites. These synapses were both symmetric (Fig. 9*d*) and asymmetric (Fig. 9*c*). Glial processes (Fig. 9*c*, asterisks) frequently separated the contact zone from the surrounding neuropil. TH-labeled terminals were commonly in apposition to unlabeled terminals, and, in one case (Fig. 9*b*), dense membrane specializations were seen between TH-labeled and unlabeled terminals.

Discussion

We have made the following observations in the rat VTA.

1. Tyrosine hydroxylase-like immunoreactivity (THLI) is localized in nuclei and cytoplasm of neuronal perikarya and dendrites containing usual, as well as unusual, organelles and exhibiting several types of junctions.

2. The cytoplasmic, but not nuclear, density of THLI in perikarya is correlated with the relative number of somatic synapses from unlabeled terminals.

3. Dendrites containing THLI are apposed to TH-labeled dendrites and are postsynaptic to TH-labeled terminals.

These findings are summarized in Figure 10 and are discussed relative to the possible functions of TH in dopaminergic neurons of the VTA.

Cytoplasmic organelles

The majority of the observed subcellular organelles in perikarya containing THLI were the same as those described previously (Domesick et al., 1983) and, thus, will not be discussed further. In addition, both intensely and lightly labeled soma and dendrites contained several unusual organelles, including cilia, lamellar bodies, and subsurface cisterns. These have been reported in other neurons from brains of many species (Henderson, 1989), including man (Cragg, 1976). The functions of these organelles in dopaminergic neurons are unknown, but they may be similar to those suggested for neurons in other brain regions.

Cilia in the VTA were identical in their microtubular arrangement to those found in other brain regions, where they have been considered as possible chemosensors (Barnes, 1961), mechanoreceptors (Allen, 1965), or vestigial remnants of a neuroepithelial ancestry (Peters et al., 1976).

Lamellar bodies have been associated with high levels of synthetic activity (King et al., 1974), particularly as relates to the production of neurosecretory products and vesicles (Cohen and Pfaff, 1981). This is of interest in view of the fact that some dopaminergic neurons of the VTA synthesize neuropeptides such as neurotensin (Hökfelt et al., 1984) and/or cholecystokinin (Hökfelt et al., 1980; Seroogy et al., 1988). Of these, neurotensin has been most clearly localized in large dense-core vesicles of dopaminergic neurons in the VTA that also contain lamellar bodies (Bayer et al., 1988). However, there is no direct evidence for the involvement of lamellar bodies in the production of neuropeptides within the VTA.

Subsurface cisterns are located immediately beneath the plasmalemma (Le Beux, 1972). These cisterns, as well as lamellae of endoplasmic reticulum have been postulated to be nonmitochondrial intercellular storage sites for calcium (McBurney and Neering, 1987). As potential calcium storage sites, subsurface cisterns may be important in the VTA, especially for burst firing of dopaminergic neurons (Grace and Bunney, 1984).

Dendritic and somatic appositions

The frequently observed appositions between TH-labeled perikarya and between 2 TH-labeled or labeled and unlabeled soma and dendrites were characterized by (1) junctions that appeared to be adhesive such as the puncta adherens (Van den Pol, 1980) and the fingerlike extensions or (2) long stretches where the membranes of the cell–cell border were in extremely close contact. The regions of close contact may indicate sites where fluorescent markers can be transferred, presumably through gap junctions, between dopaminergic perikarya in the VTA (Grace and Bunney, 1983). This possibility is supported by the multilaminar appearance of appositions between TH-IR profiles in favorable planes of section which resemble gap junctional plaques viewed in cross-section (Raviola et al., 1980). However, the classic 7-laminae array was difficult to discern in our material, possibly reflecting the fixation conditions for immunocytochemistry (Hsu et al., 1981). Despite this limitation, our data provide other indirect evidence for the presence of gap junctions between perikarya and/or dendrites. Gap junction particles are known to have a much higher turnover rate than most other plasma membrane constituents (Yancey et al., 1981), and in most cases of apposition between somata, numerous membrane-bound saccules were present on both sides of the plasmalemmal interface. These saccules were much larger than typical synaptic vesicles, 40–100 nm (Pappas and Waxman, 1972). Additionally, they were seen in apparent fusion with the plasmalemma and were sometimes coated (Pierce and Lindskog, 1988). Cisterns of endoplasmic reticulum were also found near the appositional zones, suggesting a high rate of synthetic activity. The observed ultrastructural features of appositional zones, as well as nearness of nuclei to them suggests a morphological basis for nonsynaptic, cell–cell communication between 2 TH-labeled or labeled and unlabeled perikarya and/or dendrites in the VTA. Such communication may involve transfer of intracellular regulatory, electrical, or chemical signals.

Regulatory signals. Regulatory chemical signals such as cyclic AMP may pass between cells through gap junctional channels or via membrane bound vesicles, to act as nuclear second messengers (Kurosawa et al., 1979). Alternatively, contact-mediated factors could themselves cause biochemical changes resulting in new protein synthesis similar to what has recently been shown for noradrenergic neurons in the peripheral sympathetic ganglia (Adler et al., 1989).

Electrical signals. Electrical signals would involve the transfer of ions across apposed cell membranes, most likely through gap junctions. The ultrastructural observations of close cell–cell appositions and prominence of organelles believed to be associated with calcium storage could provide a cellular basis for the rapid transcellular depolarization shown electrophysiologically in the VTA (Bunney et al., 1987), inferior olive (Sotelo and Korn, 1978), and other regions. These regions engage in burst firing, where there is a need for cell recruitment. Burst firing involves neurons firing in near synchrony (Grace and Bunney, 1983). This near synchrony would be most readily elicited by electrotonic coupling (Getting and Willows, 1974) and by dual synaptic inputs between neurons as seen in the VTA.

Chemical signals. Chemical signals may be transmitted at sites of apposition between TH-labeled profiles by release of dopamine or other coexisting neurotransmitters. The possibility of dendritic release of dopamine is supported by *in vivo* micro-

dialysis (Kalivas et al., 1989) and antidromic stimulation of the median forebrain bundle (Korf et al., 1976), showing that dopamine is released by dendrites of VTA neurons. Similarly, in the substantia nigra dopamine is stored (Bjorklund and Lindvall, 1975) and released (Geffen et al., 1976) to inhibit tonically active dopaminergic neurons in the area (Wang, 1981). Inhibition by dendritically released dopamine may provide at least one substrate for autoinhibition (Wilson et al., 1977) and the close appositions found between TH-immunoreactive dendrites would be consistent with this view. Although dendrites and perikarya contained few smooth clear vesicles and dense-core vesicles on their presumed presynaptic sides, even a few vesicles may release dopamine or other coexisting products such as cholecystokinin or neurotensin (Bartfai, 1985). These peptides are found in dense-core vesicles in dopaminergic neurons of the VTA and are modulatory to dopaminergic neurons (Quirion, 1983; Studler et al., 1985).

Nuclear THLI

TH or a structurally similar molecule was detected in varying amounts in nuclei of perikarya showing cytoplasmic labeling in the VTA. Several methodological factors might account for the unexpected detection of THLI in these nuclei. First, TH is a soluble enzyme (Nagatsu et al., 1964; Musacchio, 1968) and, thus, may have diffused into the nuclei from the cytoplasm during the processing of tissue for immunocytochemistry. However, the observation that perikarya with intense cytoplasmic labeling do not necessarily exhibit more intense nuclear labeling than neurons with light cytoplasmic labeling casts doubt on this possibility. Second, the antiserum to TH could recognize some nonspecific protein found in the nucleus (Schilling et al., 1989). This, too, seems unlikely since nuclei of nondopaminergic neurons in neighboring cell groups were unlabeled. The detected nuclear THLI also may reflect the presence of TH or a similarly antigenic substance that is selectively active in dopaminergic neurons. This possibility is supported by the intense immunoreactivity associated with the outer leaflets of the nuclear envelope, where the influx of TH-related products might occur (Broadwell and Cataldo, 1983). The close proximity between nuclei and somatosomatic appositions would provide an ideal substrate for potential interactions between the biochemical and nuclear machinery of adjacent cells as discussed above.

The nuclear labeling for TH in the VTA is similar to the observed labeling with antibody to phenylethanolamine-*N*-methyl transferase (PNMT) of adrenergic neurons in the rostral ventrolateral medulla (Milner et al., 1987). Nuclear THLI was not detected in these PNMT-containing perikarya; thus, the last enzyme in the catecholamine synthetic pathway, TH in dopaminergic neurons and PNMT in adrenergic ones (Nagatsu et al., 1964; Hökfelt et al., 1974), might subserve some feedback function in the nucleus, where transcription of genes coding for the specifically needed enzymes in the pathway occurs (Lewin, 1985). It must be stated, however, that such a function for TH has yet to be shown.

Cytoplasmic variations of THLI

Since detected immunoreactivity diminishes with increased depth due to decreasing antibody penetration (Pickel, 1986; Pickel et al., 1986), the detected variations in cytoplasmic THLI could be attributed to differences in location of identified profiles relative to the surface of the tissue. However, this is unlikely, as all samples used for numerical analysis were taken from the extreme outer surface of the tissue. Moreover, the relative constancy in the ratio of intensely versus lightly labeled profiles in 4 size categories, ranging from soma to distal dendrites, indicates that differences in detected immunoreactivity are probably not due to differences in penetration. Differences attributed to factors such as penetration also would not be expected to show differences with respect to synaptic input or differences in occurrence of appositions with other labeled or unlabeled soma or dendrites, as seen in the present study. Within the total population of neurons of the VTA, THLI showed a broad range of densities. However, reaction product was present in sufficiently different densities to permit the distinction of neighboring soma and dendrites as lightly or intensely immunoreactive by both PAP and immunoautoradiographic methods. The intensely immunoreactive soma and dendrites were (1) more numerous, (2) received more single and convergent input from unlabeled terminals, and (3) showed somewhat more frequent somatic and dendritic appositions. These findings are discussed in terms of their possible implications both for TH and for the cell as a whole.

Neurons displaying relatively denser reaction product may contain either greater quantities of TH or relatively more activated TH than the neurons with less dense reaction product. A correlation between immunoreactivity and amount of TH enzyme present in the cells of the locus coeruleus has been shown (Benno et al., 1982). Thus, our more intensely labeled cells may possess more TH enzyme than the more lightly labeled ones. Alternatively, increases in TH mRNA and enzymatic activity have been observed after transsynaptic stimulation of the sympathetic ganglion and can be abolished by nerve transection (Black et al., 1985). If such stimulation allows for an increase in TH activity, then the intensely labeled cells, having more inputs and, thus, more chances for stimulation, may have more TH activity than the more lightly labeled variety. Immunoreactivity in the present study also may represent the catalytically active portions of the enzyme because the antiserum was prepared against the trypsin-treated form of TH (Joh and Ross, 1983). The trypsin-treated form has most, if not all, regulatory sites (phosphorylation sites) removed (Zigmond et al., 1989).

Neurons containing relatively more detectable THLI may be physiologically more active. One-third to one-half of dopaminergic neurons in the rat do not fire without stimulation (Bunney and Grace, 1978). Since the more numerous intensely labeled perikarya have a greater density of synaptic inputs than lightly labeled perikarya, it is likely that they would receive more frequent stimulation. Some neurons with more intense THLI might also be involved in burst firing. With diminished synaptic input, as seen in slice preparations, burst firing is abolished in neurons of the VTA (Mueller and Brodie, 1989). More intense THLI staining would also be consistent with the observation that burst firing may release more dopamine than is released when neurons fire singly (Grace, 1988).

Afferent input from TH-labeled terminals

The major targets of TH-labeled terminals in the VTA were dendrites also labeled for the enzyme. These dendrites labeled with TH are presumed to be dopaminergic since no other catecholamines are known to be present in intrinsic neurons of the VTA (Bjorklund and Nobin, 1973; Swanson and Hartman, 1975). However, the THLI terminals may contain dopamine or other

catecholamines such as noradrenaline. Noradrenergic terminals are found in the VTA (Lindvall and Björklund, 1974) and are most likely derived from the locus coeruleus (Simon et al., 1979). In contrast, dopaminergic terminals may be derived locally from A10 neurons or from projections of the A8 (Deutch et al., 1988) or other groups of dopaminergic cells. Both dopamine and noradrenaline cause an inhibition of DA cell firing when iontophoresed into the VTA (White and Wang, 1984). Additionally, noradrenaline appears to exert an excitatory influence, perhaps indirectly, on dopaminergic neurons in the mesocortical pathway of the VTA (Herve et al., 1982). The results of this study provide anatomical support for catecholaminergic (dopaminergic and/or noradrenergic) modulation of dopamine neurons in the VTA through direct axodendritic junctions. The small number of axodendritic as opposed to dendrodendritic junctions between TH-labeled profiles may indicate more difficulty in immunolabeling small axon terminals or the more prominent role of dendritic associations in dopaminergic modulation of dopamine neurons within the VTA.

References

Abdel-Akher M, Hamilton JK, Montgomery R, Smith F (1952) A new procedure for the demonstration of the fine structure polysaccharide. J Am Chem Soc 74:4970–4971.

Adler JE, Schleifer LS, Black IB (1989) Partial purification and characterization of a membrane-derived factor regulating neurotransmitter phenotypic expression. Proc Natl Acad Sci USA 86:1080–1083.

Allen RA (1965) Isolated cilia in inner retinal neurons and in retinal pigment epithelium. J Ultrastruct Res 12:730–747.

Barnes BG (1961) Ciliated secretory cells in the pars distalis of the monkey hypophysis. J Ultrastruct Res 5:453–467.

Bartfai T (1985) Presynaptic aspects of the coexistence of classical neurotransmitters and peptides. Trends Pharmacol Sci 6:331–334.

Bayer VE, Pickel VM, Towle AC (1988) Ultrastructural localization of neurotensin in the ventral tegmental area and central nucleus of the amygdala. Soc Neurosci Abstr 14:670.

Beaudet A, Descarries L (1986) Ultrastructural identification of serotonin neurons. In: Ultrastructural identification of monoamine neurons (Furness J, Costa M, eds). London: Wiley.

Benno RH, Tucker LW, Joh TH, Reis DJ (1982) Quantitative immunocytochemistry of tyrosine hydroxylase in rat brain. II. Variations in the amount of tyrosine hydroxylase among individual neurons of the locus coeruleus in relationship to neuronal morphology and topography. Brain Res 246:237–247.

Bjorklund A, Lindvall O (1975) Dopamine in dendrites of substantia nigra neurons: suggestions for a role in dendritic terminals. Brain Res 83:531–537.

Bjorklund A, Nobin A (1973) Fluorescence histochemical and microspectrofluorometric mapping of dopamine and noradrenaline cell groups in the rat diencephalon. Brain Res 51:193–205.

Black IB, Chikaraishi DM, Lewis EJ (1985) Transsynaptic increase in RNA coding for tyrosine hydroxylase in a rat sympathetic ganglion. Brain Res 339:151–153.

Broadwell RD, Cataldo AM (1983) The neuronal endoplasmic reticulum: its cytochemistry and contribution to the endomembrane system. J Histochem Cytochem 31:1077–1088.

Bunney BS, Grace AA (1978) Acute and chronic haloperidol treatment: comparison of effects on nigral dopaminergic cell activity. Life Sci 23:1715–1728.

Bunney BS, Sesack SR, Silva NL (1987) Midbrain dopaminergic systems: neurophysiology and electrophysiological pharmacology. In: Psychopharmacology: the third generation of progress (Meltzer HY, ed), pp 113–126. New York: Raven.

Cohen RS, Pfaff DW (1981) Ultrastructure of neurons in the ventromedial nucleus or the hypothalamus in ovariectomized rats with or without estrogen treatment. Cell Tissue Res 217:451–470.

Cragg BG (1976) Ultrastructural feature of human cerebral cortex. J Anat 121:331–362.

Crow TJ (1972) Catecholamine-containing neurones and electrical self-stimulation. 1. A review of some data. Psychol Med 2:414–421.

Dahlstrom A, Fuxe K (1964) Evidence for the existence of monoamine containing neurons in the central nervous system. I. Demonstration of monoamines in the cell bodies of brain stem neurons. Acta Physiol Scand 232:1–55.

Deutch AY, Goldstein M, Baldino F, Jr, Roth RH (1988) Telencephalic projections of the A8 dopamine cell group. Ann NY Acad Sci 537:27–50.

Domesick VB, Stinus L, Paskevich PA (1983) The cytology of dopaminergic and nondopaminergic neurons in the substantia nigra and ventral tegmental area of the rat: a light- and electron-microscopic study. Neuroscience 8:743–765.

Geffen LB, Jessel TM, Cuello AC, Iversen LL (1976) Release of dopamine from dendrites in rat substantia nigra. Nature 260:258–260.

Getting, PA, Willows AOD (1974) Modification of neuron properties of electrotonic synapses. II. Burst formation by electrotonic synapses. J Neurophysiol. 37:858–868.

Grace AA (1988) *In vivo* and *in vitro* intracellular recordings from rat midbrain dopamine neurons. Ann NY Acad Sci 537:51–76.

Grace AA, Bunney BS (1983) Intracellular and extracellular electrophysiology of nigral dopaminergic neurons-3. Evidence for electrotonic coupling. Neuroscience 10:333–348.

Grace AA, Bunney BS (1984) The control of firing pattern in nigral dopamine neurons: burst firing. J Neurosci 4:2877–2890.

Henderson Z (1989) Lamellar bodies are markers of cholinergic neurons in ferret nucleus basalis. J Neurocytol 18:95–103.

Herve D, Blanc G, Glowinski J, Tassin JP (1982) Reduction of dopamine utilization in the prefrontal cortex but not in the nucleus accumbens after selective destruction of noradrenergic fibers innervating the ventral tegmental area in the rat. Brain Res 237:510–516.

Herve D, Pickel VM, Joh TH, Beaudet A (1987) Serotonin axon terminals in the ventral tegmental area of the rat: fine structure and synaptic input to dopaminergic neurons. Brain Res 435:71–83.

Hökfelt T, Fuxe K, Goldstein M, Johansson O (1974) Immunohistochemical evidence for the existence of adrenaline neurons in the rat brain. Brain Res 66:235–251.

Hökfelt T, Johansson O, Fuxe K, Goldstein M, Park DH (1976) Immunohistochemical studies on the localization and distribution of monoamine neuron systems in the rat brain. I. Tyrosine hydroxylase in the mesencephalon. Med Biol 54:427–453.

Hökfelt T, Rehfeld JF, Skirboll L, Ivemark B, Goldstein M, Markey K (1980) Evidence for coexistence of dopamine and CCK in mesolimbic neurones. Nature 285:476–478.

Hökfelt T, Everitt BJ, Theodorsson-Norheim E, Goldstein M (1984) Occurrence of neurotensinlike immunoreactivity in subpopulations of hypothalamic mesencephalic and medullary catecholamine neurons. J Comp Neurol 222:543–559.

Hsu S-M, Raine L, Fanger H (1981) The use of avidin-biotin-peroxidase complex (ABC) in immunoperoxidase techniques: a comparison between ABC and unlabeled antibody (peroxidase) procedures. J Histochem Cytochem 29:577–580.

Joh TH, Ross ME (1983) Preparation of catecholamine-synthesizing enzymes as immunogens for immunohistochemistry. In: Methods in neuroscience: immunohistochemistry (Cuello AC, ed), pp 121–138. Chichester, UK: IBRO.

Kalivas PW, Bourdelais A, Abhold R, Abbott L (1989) Somatodendritic release of endogenous dopamine: in vivo dialysis in the A10 dopamine region. Neurosci Lett 100:215–220.

King JC, Williams TH, Gerall AA (1974) Transformations of hypothalamic arcuate neurons. I. Changes associated with stages of the estrous cycle. Cell Tissue Res 153:497–515.

Korf J, Zieleman M, Westerink BHC (1976) Dopamine release in substantia nigra? Nature 260:257–258.

Kurosawa A, Guidotti A, Costa E (1979) Nuclear translocation of cyclic AMP-dependent protein kinase subunits during the transsynaptic activation of gene expression in rat. Mol Pharmacol 15:115–130.

Le Beux YJ (1972) Subsurface cisterns and lamellar bodies: particular forms of the endoplasmic reticulum in the neurons. Z Zellforsch Mikrosk Anat 133:327–352.

Lewin B (1985) Genes II, 2nd ed. New York: Wiley.

Lindvall O, Bjorklund A (1974) The organization of the ascending catecholamine neuron systems in the rat brain as revealed by the glyoxylic acid fluorescence method. Acta Physiol Scand Suppl 412: 1–48.

McBurney RN, Neering IR (1987) Neuronal calcium homeostasis. Trends Neurosci 10:164–169.

Milner TA, Pickel VM, Park DH, Joh TH, Reis DJ (1987) Phenylethanolamine N-methyltransferase-containing neurons in the rostral ventrolateral medulla of the rat. I. Normal ultrastructure. Brain Res 411: 28–45.

Mogenson GJ, Wu M, Manchanda SK (1979) Locomotor activity initiated by microinfusion of picrotoxin into the ventral tegmental area. Brain Res 161:311–319.

Mueller AL, Brodie MS (1989) Intracellular recording from putative dopamine-containing neurons in the ventral tegmental area of Tsai in a brain slice preparation. J Neurosci Methods 28:15–22.

Musacchio JM (1968) Subcellular distribution of adrenal tyrosine hydroxylase. Biochem Pharmacol 17:1470–1473.

Nagatsu T, Levit M, Udenfriend S (1964) Tyrosine hydroxylase: the initial step in norepinephrine biosynthesis. J Biol Chem 239:2910–2917.

Oades RD, Halliday GM (1987) Ventral tegmental (A10) system: neurobiology. 1. Anatomy and connectivity. Brain Res Rev 12:117–165.

Ordronneau P, Lindstrom PBM, Petrusz P (1981) Four unlabled antibody bridge techniques. A comparison. J Histochem Cytochem 29: 1397–1404.

Papp M, Bal A (1986) Motivational versus motor impairment after haloperidol injection or 6-OHDA lesions in the ventral tegmental area or substantia nigra in rats. Physiol Behav 38:773–779.

Pappas GD, Waxman SG (1972) Synaptic fine structure—morphological correlates of chemical and electrotonic transmission. In: Structure and function of synapses (Pappas GD, Purpura DP, eds), pp 1–43. New York: Raven.

Paxinos G, Watson C (1986) The rat brain in stereotaxic coordinates. Orlando, FL: Academic.

Peters A, Palay SL, Webster HdF (1976) The fine structure of the nervous system: the neurons and supporting cells, pp 90–117. Philadelphia: Saunders.

Phillipson OT (1979a) Afferent projections to the ventral tegmental area of Tsai and interfascicular nucleus: a horseradish peroxidase study in the rat. J Comp Neurol 187:117–144.

Phillipson OT (1979b) The cytoarchitecture of the interfascicular nucleus and ventral tegmental area of Tsai in the rat. J Comp Neurol 187:85–98.

Piazza PV, Ferdico M, Russo D, Crescimanno G, Benigno A, Amato G (1988) Facilitatory effect of ventral tegmental area A10 region on the attack behaviour in the cat: possible dopaminergic role in selective attention. Exp Brain Res 72:109–116.

Pickel VM (1986) Ultrastructure of central catecholaminergic neurons. In: Neurohistochemistry: modern methods and applications, Vol 16 (Panula P, Paivarinta H, Somila S, eds), pp 397–423. New York: Liss.

Pickel VM, Chan J, Milner TA (1986) Autoradiographic detection of (^{125}I)-secondary antiserum: a sensitive light and electron microscopic labeling method compatible with peroxidase immunocytochemistry for dual localization of neuronal antigens. J Histochem Cytochem 34: 707–718.

Pierce A, Lindskog S (1988) Coated pits and vesicles in the osteoclast. J Submicrosc Cytol Pathol 20:161–167.

Quirion R (1983) Interactions between neurotensin and dopamine in the brain: an overview. Peptides 4:609–615.

Raviola E, Goodenough A, Raviola G (1980) Structure of rapidly frozen gap junctions. J Cell Biol 87:273–279.

Schilling K, Duvernoy C, Keck S, Pilgrim C (1989) Detection and partial characterization of a developmentally regulated nuclear antigen in neural cells in vitro and in vivo. J Histochem Cytochem 37: 241–247.

Seroogy K, Ceccatelli S, Schalling M, Hökfelt T, Frey P, Walsh J, Dockray G, Brown J, Buchan A, Goldstein M (1988) A subpopulation of dopaminergic neurons in the rat mesencephalon contains both neurotensin and cholecystokinin. Brain Res 455:88–98.

Simon H, LeMoal M, Calas A (1979) Efferents and afferents of the ventral tegmental-A10 region studied after local injection of [3H] leucine and horseradish peroxidase. Brain Res 178:17–40.

Simon H, Scatton B, Le Moal M (1980) Dopaminergic A10 neurones are involved in cognitive functions. Nature 286:150–152.

Sotelo, C, Korn H (1978) Morphological correlates of electrical and other interactions through low resistance pathways between neurons of the vertebrate central nervous system. Int Rev Cytol 55:67–107.

Sternberger LA (1979) Immunocytochemistry. In: Basic and clinical immunology, 2nd ed (Cohen S, McClusky RT, eds). New York: Wiley.

Studler JM, Reibaud M, Tramu G, Blanc G, Glowinski J, Tassin JP (1985) Distinct properties of cholecystokinin-8 and mixed dopamine-cholecystokinin-8 neurons innervating the nucleus accumbens. Ann NY Acad Sci 448:306–314.

Swanson LW, Hartman BK (1975) The central adrenergic system. An immunofluorescence study of the location of cell bodies and their efferent connections in the rat utilizing dopamine-beta-hydroxylase as a marker. J Comp Neurol 163:467–505.

Taxi J (1961) Etude de l'ultrastructure des zones synaptiques dans les ganglions sympatiques de la grenouille. CR Acad Sci (Paris) 252:174–176.

Van den Pol AN (1980) The hypothalamic suprachiasmatic nucleus of rat: intrinsic anatomy. J Comp Neurol 191:661–702.

Vincent SR (1988) Distributions of tryosine hydroxylase-, dopamine-beta-hydroxylase-, and phenylethanolamine-N-methyltransferase-immunoreactive neurons in the brain of the hamster (*Mesocricetus auratus*). J Comp Neurol 268:584–599.

Wang RY (1981) Dopaminergic neurons in the rat ventral tegmental area. II. Evidence for autoregulation. Brain Res Rev 3:141–151.

White FJ, Wang RY (1984) Pharmacological characterization of dopamine autoreceptors in the rat ventral tegmental area: microiontophoretic studies. J Pharmacol Exp Ther 231:275–280.

Wilson CJ, Groves PM, Fifkova E (1977) Monoaminergic synapses, including dendro-dendritic synapses in the rat substantia nigra. Exp Brain Res 30:161–174.

Yancey SB, Nicholson BJ, Revel JP (1981) The dynamic state of liver gap junctions. J Supramol Cell Biochem 16:221–232.

Zigmond RE, Schwarzschild MA, Rittenhouse AR (1989) Acute regulation of tyrosine hydroxylase by nerve activity and by neurotransmitters via phosphorylation. Annu Rev Neurosci 12:415–461.